BNL-220627-2020-JAAM

Designing Advanced In Situ Electrode/Electrolyte Interphases for Wide Temperature Operation of 4.5 V Li||LiCoO2 Batteries

X. Ren, Z. Shadike

To be published in "Advanced Materials"

November 2020

Chemistry Department

Brookhaven National Laboratory

U.S. Department of Energy

USDOE Office of Energy Efficiency and Renewable Energy (EERE), Vehicle Technologies Office (EE-3V)

DISCLAIMER

Designing Advanced In Situ Electrode/Electrolyte Interphases for Wide Temperature Operation of 4.5 V Li||$LiCoO_2$ Batteries

Xiaodi Ren, Xianhui Zhang, Zulipiya Shadike, Lianfeng Zou, Hao Jia, Xia Cao, Mark H. Engelhard, Bethany E. Matthews, Chongmin Wang, Bruce W. Arey, Xiao-Qing Yang, Jun Liu, Ji-Guang Zhang, and Wu Xu**

High-energy-density batteries with a $LiCoO_2$ (LCO) cathode are of significant importance to the energy-storage market, especially for portable electronics. However, their development is greatly limited by the inferior performance under high voltages and challenging temperatures. Here, highly stable lithium (Li) metal batteries with LCO cathode, through the design of in situ formed, stable electrode/electrolyte interphases on both the Li anode and the LCO cathode, with an advanced electrolyte, are reported. The LCO cathode can deliver a high specific capacity of ≈190 mAh g^{-1} and show greatly improved cell performances under a high charge voltage of 4.5 V (even up to 4.55 V) and a wide temperature range from −30 to 55 °C. This work points out a promising approach for developing Li||LCO batteries for practical applications. This approach can also be used to improve the high-voltage performance of other batteries in a broad temperature range.

Lithium (Li)-ion batteries (LIBs) have enjoyed great success since their commercialization in 1991 as the preferred energy storage system in portable electronics and, more recently, in electric vehicles.[1] Nevertheless, the advancement of LIBs has fallen far behind the ever-growing needs for high-energy-density batteries nowadays. Therefore, developing high-voltage batteries with high capacity electrode materials is of critical importance for future applications. Among various commercial cathode materials, $LiCoO_2$ (LCO) has been an essential member since its discovery in 1980s and still possesses many competitive advantages in the cathode material family, including high theoretical capacity, high output voltage, high Li^+ and electron conductivity, and high tap density.[2,3]

However, the practical capacity of LCO has been limited to ≈140 mAh g^{-1}, only half of its theoretical value of 275 mAh g^{-1}, under the charging cut-off voltage of 4.2 V in early developments of LCO-based batteries. Although higher cut-off voltages bring higher capacities, it is usually accompanied with serious capacity fading and performance deterioration. Beyond 4.2 V, LCO could go through bulk phase deformations to cause fast capacity fading. It should be noted that, recent studies point out that the surface degradation is an even more pressing issue for LCO cathodes cycled under higher voltages.[4] Due to the high degree of Co_{3d}—O_{2p} hybridization, electron extraction from both Co^{3+} and O^{2-} would happen in deeply delithiated LCO (above ≈150 mAh g^{-1}), which could cause O^{2-} oxidation and thus oxygen loss from the cathode.[5,6] In addition, the formation of highly oxidative Co^{4+} during charging promotes electrolyte decomposition, and the corrosive side products (e.g., HF) in conventional $LiPF_6$/carbonate electrolytes could also destabilize the LCO surface to induce Co and O loss. More importantly, the surface degradation can propagate inside the bulk particle due to the migration of oxygen vacancies.[6,7] Such effects would be more aggravated under higher temperatures due to the accelerated interfacial side reactions. Therefore, a highly stable cathode-electrolyte interphase (CEI) is indispensable for improving the LCO performance under high voltages. Although different doping/surface coating methods or electrolyte additives/salts have shown improved LCO cycling stabilities at high voltages, few reports have demonstrated feasibility for applications under elevated temperatures with charging cut-off voltage as high as 4.5 V.[3,8] Moreover, forming a favorable CEI in situ via electrolyte design is highly beneficial for practical applications, thus

Dr. X. Ren[+], Dr. X. Zhang, Dr. H. Jia, Dr. X. Cao, Dr. B. E. Matthews, Dr. B. W. Arey, Dr. J. Liu, Dr. J.-G. Zhang, Dr. W. Xu
Energy and Environment Directorate
Pacific Northwest National Laboratory
Richland, WA 99354, USA
E-mail: jiguang.zhang@pnnl.gov; wu.xu@pnnl.gov
Dr. Z. Shadike, Dr. X.-Q. Yang
Chemistry Division
Brookhaven National Laboratory
Upton, NY 11973, USA
Dr. L. Zou, M. H. Engelhard, Dr. C. Wang
Environmental Molecular Sciences Laboratory
Pacific Northwest National Laboratory
Richland, WA 99354, USA

[+]Present address: Department of Materials Science and Engineering, University of Science and Technology of China, Hefei, Anhui 230026, China

circumventing the easy failure of brittle exterior coating layers during mechanical processing or long-term cycling.[9]

The development of suitable high-voltage electrolytes for LCO becomes even more stringent when we want to maximize the energy density of LCO-based batteries by employing Li metal as the anode.[10] As an ideal anode material, Li metal presents one of the highest specific capacities of 3860 mAh g^{-1} along with the extremely low electrochemical potential (−3.040 V vs standard hydrogen electrode). However, its notoriously high reactivity toward electrolytes causes significant obstacles for battery applications: severe side reactions, quick consumption of Li metal and electrolyte, Li dendrite growth, etc.[11] Therefore, in order to achieve a high-energy-density Li‖LCO battery with good performance for practical applications, it is of critical importance to find electrolytes satisfying the following criteria: 1) highly stable with the Li metal anode, 2) highly stable with the LCO under high voltages, 3) capable of operating in a wide-temperature range, and 4) suitable for high-rate conditions. Recently, significant progresses have been made by using localized high-concentration electrolytes (LHCEs) to enhance the cycling stability of various battery chemistries, such as Li metal batteries, Na metal batteries, Li—O_2 batteries, LIBs, etc.[12] However, the stability of LHCEs is also affected by the selection of cathode materials. Among the intercalation cathode materials such as $LiFePO_4$, $LiNi_xMn_yCo_{1-x-y}O_2$ (NMC), and LCO, LCO has high Co content and Co itself has catalytic capability that may promote more side reactions at high voltages. Therefore, further development and evaluation are critical to verify the high-voltage stability of LHCEs used for Li‖LCO batteries even some of these electrolytes have been proven to be stable with other cathode materials like NMC. In contrast to conventional ether electrolytes that are unstable beyond 4 V, ether-based LHCEs show great potential for stabilizing high-voltage cathodes, while maintaining excellent stability with Li metal, thus providing a unique electrolyte design strategy to solve the notorious Li anode challenge. Here, we demonstrate a long cycling Li‖LCO battery with a high charging voltage of 4.5 V by designing advanced electrode/electrolyte interphases on both LCO cathode and Li anode via an in situ formation process. Using a new ether-based LHCE, the Li‖LCO battery has demonstrated a discharge capacity of about 137 mAh g^{-1} after 800 cycles under 4.5 V at room temperature (RT, i.e., 25 °C), and about 82% capacity retention after 200 rigorous cycles at 55 °C.

The electrochemical performances of Li‖LCO batteries were evaluated using galvanostatic cycling within the voltage range of 3.0–4.5 V under different temperatures. A medium-high cathode loading of ≈13.5 mg cm^{-2} (or ≈2.6 mAh cm^{-2} under 4.5 V) was used to ensure that an appreciable amount of Li metal was deposited and stripped each cycle. The charge and discharge rates were 0.63 and 1.9 mA cm^{-2}, respectively. In the conventional carbonate electrolyte (1 M $LiPF_6$ in ethylene carbonate (EC)–ethyl methyl carbonate (EMC) (3:7 by volume) with 2 wt% vinylene carbonate, referred as BL-carbonate electrolyte hereafter), the Li‖LCO cell, with 450 μm thick Li and 75 μL electrolyte, shows a continuous capacity fading along with obvious overpotential increases in voltage profiles at RT (**Figure 1**a and Figure S1a, Supporting Information). The cell only exhibits a specific capacity of 64 mAh g^{-1} (36% capacity retention) after 200 cycles. The cell average Coulombic efficiency (CE) is about 99.0%, indicating there are still apparent side reactions (1.0% per cycle) on the LCO cathode and the Li anode, more specifically on the cathode because the Li metal and the electrolyte in the cells are in excess amounts. These side reactions are most likely due to the excessive oxidation of the carbonate electrolyte on LCO surface under the 4.5 V high voltage. Such a deleterious effect is more pronounced under elevated temperatures. A significantly accelerated capacity decay is observed at 45 °C and the average cell CE is even lower (97.1% for the first 100 cycles), compared to those under RT.

Nevertheless, as indicated in Figure 1b, the cycling performances of Li‖LCO cells dramatically improve when a newly formulated ether-based LHCE (referred as AD-ether electrolyte hereafter) is employed. The electrolyte consists of lithium bis(fluorosulfonyl)imide (LiFSI), 1,2-dimethoxyethane (DME) and 1,1,2,2-tetrafluoroethyl 2,2,3,3-tetrafluoropropyl ether (TTE), with a molar ratio of 1:1:3. TTE has a negligible ability to dissolve LiFSI compared to DME, thus it is rarely involved in the solvation of the salt ions. Previously, a ratio of 1:1.2 between LiFSI and DME was found to be useful for the Ni-rich $LiNi_{0.8}Mn_{0.1}Co_{0.1}O_2$ (NMC811) cathode with an upper voltage of 4.4 V.[13] Here, the higher salt/solvent ratio selected is to minimize the amount of "free" solvent DME while maintaining a good miscibility with the diluent TTE. As a result, an LHCE is formed with viscosity (3.7 cP at 25 °C) and ion conductivity (1.6 mS cm^{-1} at 25 °C) comparable to the conventional BL-carbonate electrolyte (3.8 cP and 8.3 mS cm^{-1} at 25 °C). Importantly, the cycling stability of Li‖LCO cells is dramatically improved in the AD-ether electrolyte. At RT, the cell can maintain 92.9% of the initial capacity after 300 cycles (Figure 1b). Meanwhile, the cell shows very consistent voltage profiles over the entire cycling, with minimum middle voltage drop, which implies the excellent cathode stability under high voltage in the AD-ether electrolyte (Figure S1b, Supporting Information). The greatly increased cell CE of about 99.9% suggests that the undesired side reactions between the electrolyte and the LCO cathode under high voltage are largely suppressed. Furthermore, the AD-ether electrolyte could enable superior cell cycling performances under elevated temperatures. Under 45 and 55 °C, the cell capacity retentions are 83.6% (300 cycles) and 81.3% (200 cycles), respectively. The lower cell CEs observed during earlier cycles under elevated temperatures (Figure 1b) are due to the accelerated electrolyte side reaction kinetics compared to that under RT. Nevertheless, the CEI gradually stabilizes to inhibit parasite reactions and improves the cell CEs to a high level. Overall, the AD-ether electrolyte significantly improves the Li‖LCO battery cycling performance under 4.5 V. In a separated long-term cycling test, the cell delivers a high specific capacity of 136.7 mAh g^{-1} (corresponding to ≈80% capacity retention) after cycling for 800 times under RT (charge and discharge at 0.63 and 1.9 mA cm^{-2}, respectively) without dendrite-induced cell short-circuiting (Figure 1c, where lower discharge capacities in first few cycles are likely due to the initial passivation film formation on that batch of Li metal chips). Compared to the LiFSI-1.2DME-3TTE electrolyte reported lately, the AD-ether electrolyte (LiFSI-1.0DME-3TTE) shows better anodic stability due to the reduction of "free" DME molecules (Figure S2, Supporting Information). As shown in Figures S3 and S4, Supporting Information, the AD-ether

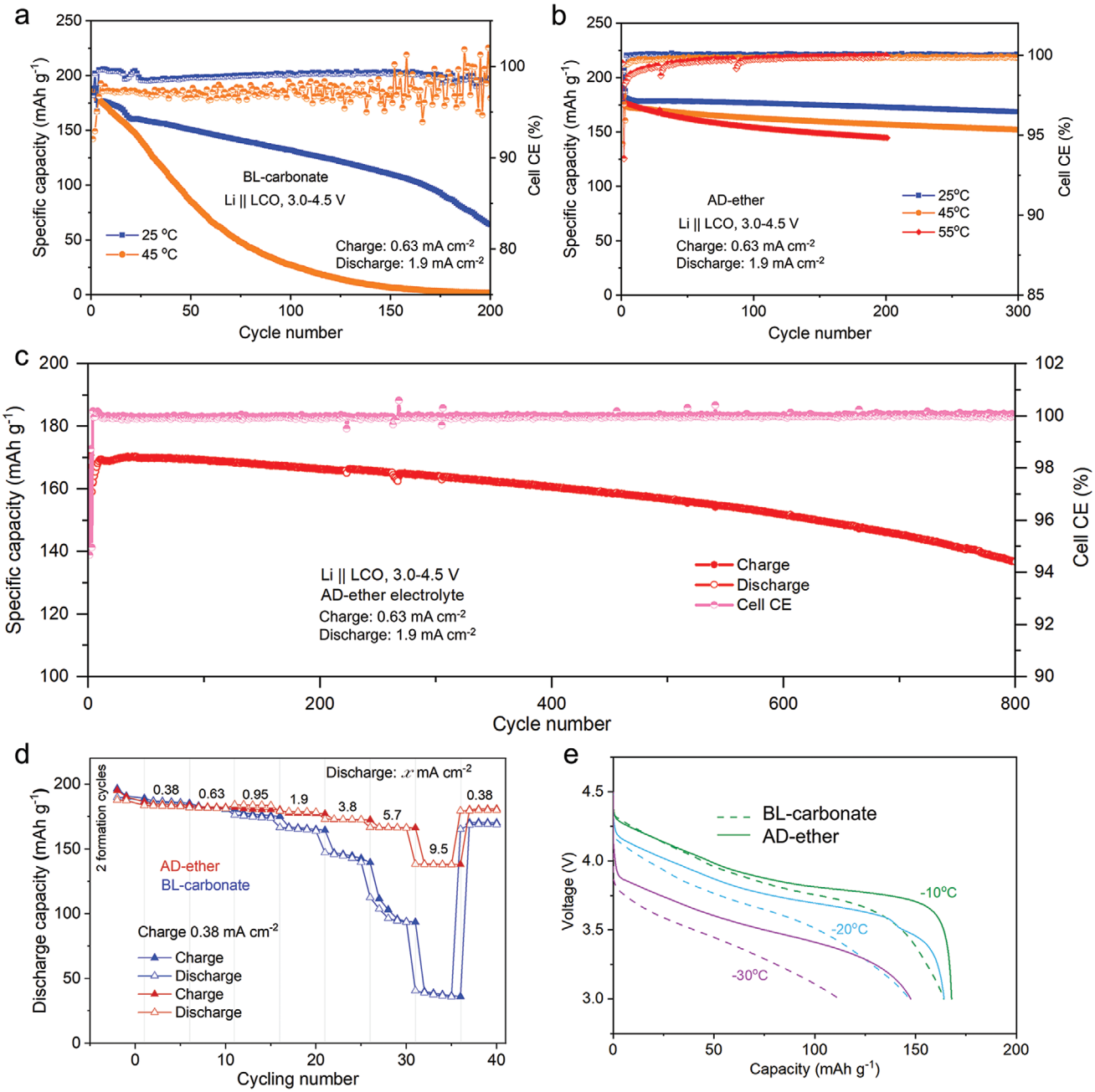

Figure 1. Electrochemical performances of Li||LCO batteries. a) Cycling performances in the BL-carbonate electrolyte at 4.5 V under RT and 45 °C. b) Cycling performances in the AD-ether electrolyte at 4.5 V under RT, 45 and 55 °C. c) Long-term cycling stability test in the AD-ether electrolyte under RT. d) Cell discharge rate capability tests at RT in different electrolytes. e) Discharge tests under low temperatures in different electrolytes.

electrolyte demonstrates much better cycling performances under high temperature (55 °C) or high voltage (4.55 V, 87.6% capacity retention after 200 cycles), compared to the previously reported LiFSI-1.2DME-3TTE electrolyte.

Besides the evaluation of the effect of the AD-ether electrolyte on the long-term cycling stability of Li||LCO cells at RT and elevated temperatures, the battery rate capability and discharge performance under low temperatures with the two electrolytes were also comparatively studied. A specific capacity of nearly 140 mAh g^{-1} can be achieved at 9.5 mA cm^{-2} discharge rate for the AD-ether electrolyte, far better than that measured in the BL-carbonate electrolyte (Figure 1d). In addition, when tested at sub-zero temperatures (–10, –20, and –30 °C), the cells with the AD-ether electrolyte exhibit apparently higher discharge capacities and average voltage outputs (Figure 1e). It is indicated that the AD-ether electrolyte not only shows excellent electrochemical stabilities with the Li metal anode and the reactive LCO cathode at high voltage and under elevated temperatures, but also improves the battery rate capability and low-temperature discharge behaviors. Therefore, the use of the AD-ether

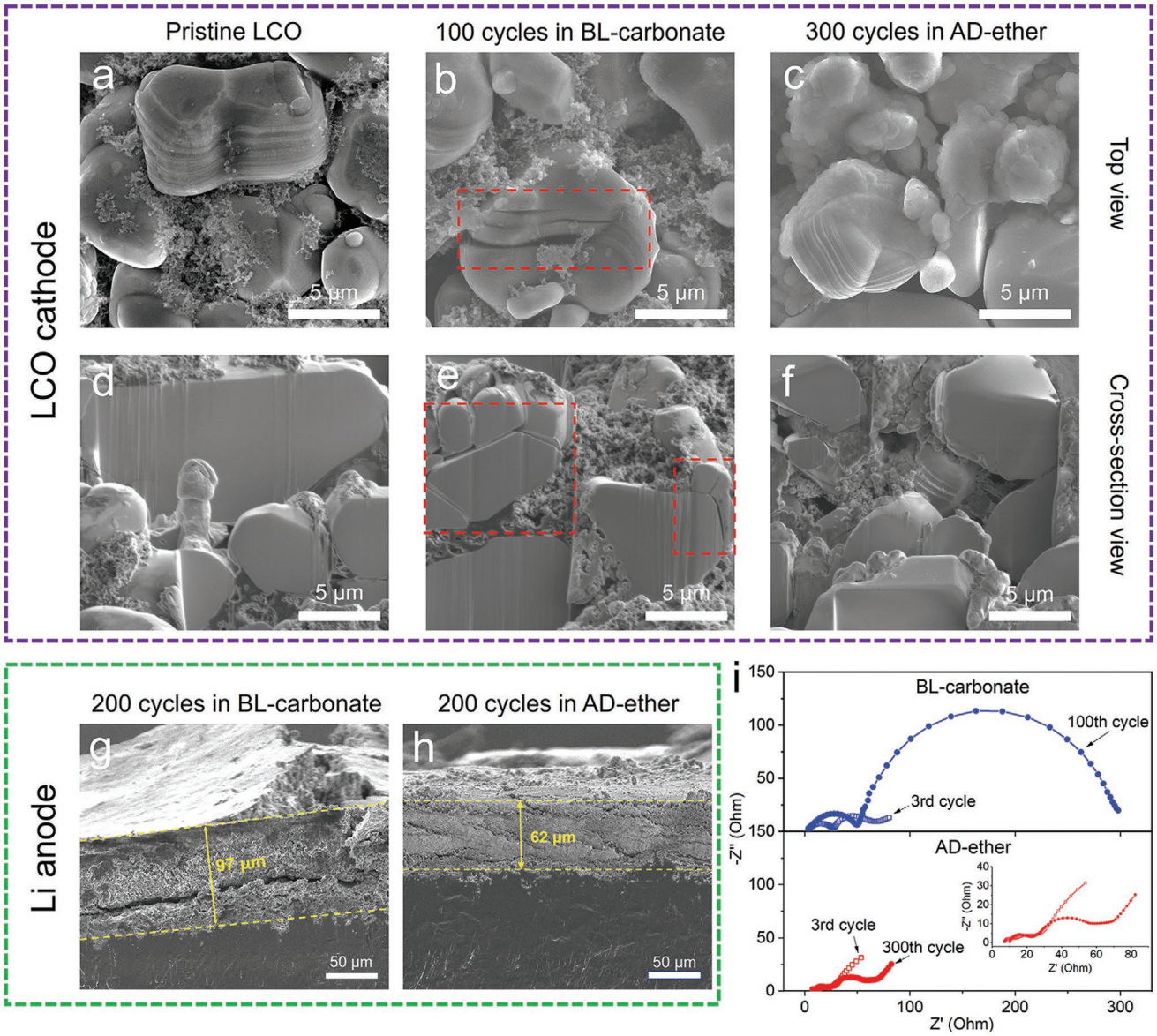

Figure 2. a–h) SEM images and i) EIS characterizations of electrodes and Li||LCO cells after cycling. a,d) The pristine LCO cathode. b,e) The LCO cathode after 100 cycles in BL-carbonate. c,f) The LCO cathode after 300 cycles in AD-ether. a–c) Top-view images. c–f) Cross-section images. g) The Li anode after 200 cycles in BL-carbonate. h) The Li anode after 200 cycles in AD-ether. i) The evolutions of cell Nyquist plots after cycling in different electrolytes.

electrolyte, instead of the conventional BL-carbonate electrolyte, addresses many critical challenges confronted with high-energy-density Li||LCO batteries and significantly promotes their practical applications.

To understand the effects of the two electrolytes on the LCO cathode and the Li anode, the cycled cells were taken part for post-analyses. The scanning electron microscopy (SEM) images at the top-view and cross-section view (prepared using focused ion beam SEM) of the pristine and cycled LCO cathodes are shown in **Figure 2**a–f. Even after just 100 cycles under 4.5 V, the LCO cathode in the BL-carbonate electrolyte develops severe cracks in bulk particles, as highlighted by the red rectangles in SEM images (Figure 2b,e). In contrast, the LCO particles in the AD-ether electrolyte are kept intact even after 300 cycles from the cross-section SEM image (Figure 2f). Part of the cathode particle is covered by a surface layer, along with exposed areas with clear textures resembling typical cathode surface. It seems that this surface layer originates from precipitates of electrolyte side products from reactions with the cathode (and/or the species generated from the anode) but does not intimately adhere to the LCO surface. On the Li anode side, the electrolyte also greatly influences the electrode stability. As seen from the cross-section image of cycled Li anodes (Figure 2g,h), side products accumulate to nearly 100 μm after 200 jeopardized cycles in the BL-carbonate electrolyte. On the contrary, the thickness of the surface layer in the AD-ether electrolyte is only ≈62 μm

after 200 cycles, suggesting suppressed side reactions between Li anode and the electrolyte. The larger particles in the surface layer in the AD-ether electrolyte also suggest the better Li anode stability (Figure S5, Supporting Information).

The prominent differences made by the electrolytes on the electrodes can be further explored by electrochemical impedance spectroscopy (EIS). As shown in Figure 2i, a major change of the Nyquist plot is found for the cell after 100 cycles in the BL-carbonate electrolyte. Both the ion diffusion impedance and charge transfer impedance (in particular) increase apparently after cycling, as indicated by the semicircles at higher frequency and lower frequency, respectively. In contrast, the impedance change in the AD-ether electrolyte is very limited even after 300 cycles under high voltage. Therefore, the AD-ether electrolyte offers significant advantages for the stabilities of both the LCO cathode and the Li anode over the BL-carbonate electrolyte.

The greatly improved Li anode stability in the AD-ether electrolyte can be mainly attributed to the favorable properties of the solid electrolyte interphase (SEI) on the Li metal surface. From the X-ray photoelectron spectroscopy (XPS) data collected on the Li anodes cycled 200 times (Figure S6, Supporting Information), the SEI in the AD-ether electrolyte shows clear evidence of preferred LiFSI salt reduction. The generation of sulfur (S)-containing components with lower binding energies (SO_x, S_n^{2-}, and Li_2S) and the enrichment of LiF suggest that the AD-ether electrolyte (as an LHCE) follows similar reactivity features with high concentration electrolytes on the Li anode.[14] Compared to excessive solvent decompositions in the BL-carbonate electrolyte, the AD-ether electrolyte switches the SEI to a "salt-dominant" chemistry. The significant presence of LiF, which possesses excellent electronic insulating capability and structure stability, can effectively protect the Li anode from further electrolyte side reactions.[15] The formation of S- and nitrogen (N)-containing anions (e.g., SO_x^{n-}, S_n^{2-}, S^{2-}, $N{-}SO_x$, etc.) may provide efficient Li^+ transport pathways because of their relatively low charge densities. Such characteristics are consistent with our previous studies of ether-based LHCEs.[13,16] Considering the excess amounts of Li metal and electrolyte used in the battery tests, the cell capacity decays should be mainly attributed to the degradation of LCO cathode under high voltage (4.5 V). This is further supported by the continued cell decay trend in the BL-carbonate electrolyte after a new Li anode and fresh electrolyte were employed, as shown in Figure S7, Supporting Information.

To further distinguish whether the bulk or the surface degradation is mainly responsible for the cathode capacity decay, X-ray diffraction (XRD) and hard X-ray absorption spectroscopy (XAS) were used to characterize the cycled cathodes. As shown in Figure S8, Supporting Information, XRD patterns of both cycled LCO cathodes indicate that the layered cathode structure is largely retained after cycling. Although the overall XRD peak intensity decreases after cycling in the BL-carbonate electrolyte, no obvious cation-mixing in the bulk structure can be found (as indicated by peak ratios of I_{003}/I_{104}, 4.2 in pristine LCO vs 5.5 in BL-carbonate). In addition, the comparison of the Co K-edge X-ray absorption near edge structure and extended X-ray absorption fine structure spectra (Figure S9, Supporting Information) indicate that the bulk LCO cathode structures show negligible changes after cycling in the BL-carbonate and the AD-ether electrolytes. Therefore, the deterioration of the LCO surface structure is mainly responsible for the cell capacity decay in the BL-carbonate electrolyte.

Aiming to understand the evolution of CEIs in the two electrolytes and its implication on cathode stability, XPS and soft XAS were employed to study the compositions on LCO cathodes. While XPS analysis is depth-sensitive only up to a few nanometers, the combination of total electron yield (TEY) mode (probing depth: ≈5 nm) and fluorescence yield (FY) mode (probing depth: ≈100 nm) analysis in XAS is able to help distinguish the surface and bulk regions and provide a more complete picture of the CEI structure. As revealed by the XPS and the soft XAS analyses (**Figure 3**), the compositions in the CEI are largely changed when switching from the BL-carbonate electrolyte to the AD-ether electrolyte. In the BL-carbonate electrolyte, the CEI on the LCO after 100 cycles is mainly composed of decomposition products from solvent molecules, as indicated by the high atomic ratios of C and O (45.92% and 34.03%, respectively, from XPS quantification) and the prominent presence of CO_3^{2-} (C 1s: 289.5 eV, O 1s: 531.6 eV). The C K-edge TEY and FY spectra of the LCO in BL-carbonate (Figure 3d and Figure S10a, Supporting Information, respectively) also confirm the enrichments of CO_3^{2-} and −COOH species in the CEI. This is also supported by the TEY and FY data for the O K-edge shown in Figure 3f and Figure S10c, Supporting Information, respectively. Two major changes are observed in O K-edge spectra of cycled LCO sample: decrease of the pre-edge peak below ≈532 eV and formation of a new shoulder peak at a higher energy ≈534 eV. The pre-edge peaks below ≈532 eV correspond to the transition of oxygen 1s electron to the hybridized state of Co 3d and O 2p orbitals. Therefore, decrease in the pre-edge intensity, especially for LCO cycled in BL-carbonate, may be caused by formation of rock-salt/spinel phases due to the surface reconstruction or formation of various organic/inorganic CEI due to the electrolyte decomposition. It is worthwhile to note that an intense peak at higher energy in O K-edge of LCO sample cycled in BL-carbonate can be observed, which is a typical signature of the CO_3^{2-} in Li_2CO_3. CO_3^{2-} and −COOH species are very likely generated from the oxidation of EC molecules on the LCO surface under high voltage. These species could further promote the decomposition of $LiPF_6$ and result in corrosive acidic products (e.g., HF).[17] Nevertheless, in the AD-ether electrolyte, the atomic ratio of F (37.98%) becomes the highest among all elements (also much higher than that in the BL-carbonate, F 7.25%), while those of C and O decrease to 30.57% and 7.61%, respectively. In addition, the chemical nature of F species on two cycled LCO cathodes have featured differences. The sole source of F in the BL-carbonate electrolyte is $LiPF_6$, whose decomposition is responsible for the formation of LiF and $PO_xF_y^{n-}$, but this is always accompanied with the cathode corrosion. In contrast, both FSI^- (salt anion) and TTE (diluent) could contribute to the formation of the F-enriched CEI in the AD-ether electrolyte, as suggested in our previous study.[13] Apart from the PVDF binder, the C-F signal could also come from the decomposition of TTE molecules. The insulating nature and the structural stability of the enriched LiF phase in the CEI in the AD-ether is also critical for the excellent performance of LCO cathode. It is interesting to note that not

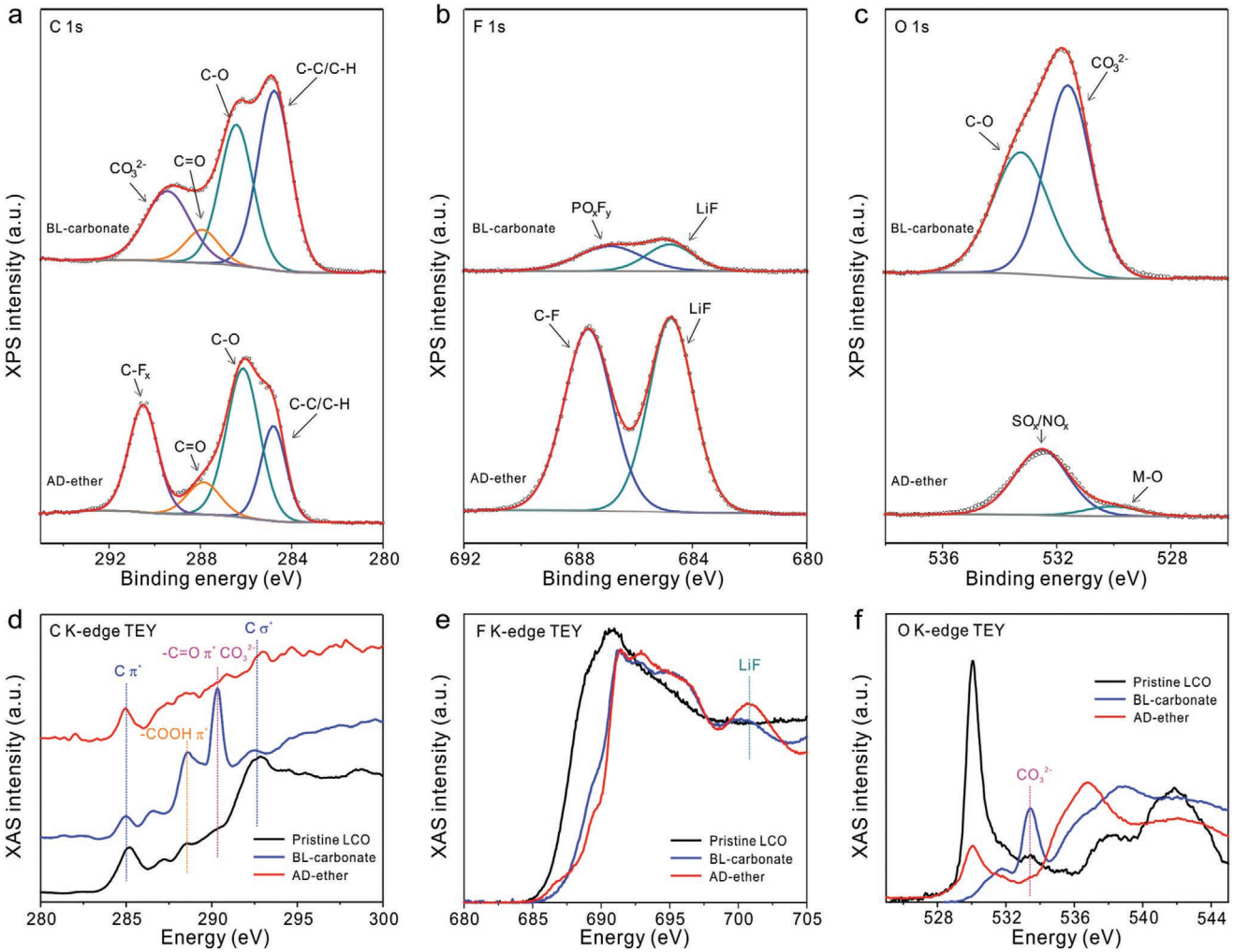

Figure 3. Compositions in the LCO/electrolyte interphases in different electrolytes by XPS and XAS measurements. a–c) C 1s, F 1s, and O 1s XPS spectra of LCO cathodes after 200 cycles. d–f) C K-edge, F K-edge, and O K-edge XAS TEY spectra of LCO cathodes after 100 cycles in BL-carbonate and 300 cycles in AD-ether, respectively.

only the relative intensity of LiF (Figure S11a, Supporting Information) increases over cycling, but the C—F signal shifts to a lower binding energy with lower intensity (Figure S11b, Supporting Information). This implies the conversion from C—F species to LiF within the CEI, which is believed to be beneficial for enhancing the long-term cathode stability. Formation of LiF-rich CEI in AD-ether is also clearly observed from TEY and FY spectra of F k-edge as shown in Figure 3b and Figure S10b, Supporting Information. The F K-edge spectrum of the pristine sample is contributed by the PVDF binder. For the sample cycled in the AD-ether electrolytes, a small shoulder peak forms at ≈700 eV and the edge shifts to higher energy significantly, which is close to the edge of LiF.[18] Although the F K-edge of LCO sample cycled in BL-carbonate shifts toward high energy, the energy is still lower than that of cycled in AD-ether electrolyte, suggesting that the F compounds detected in F K-edge XAS are mixture of LiF, PVDF, and PO_xF_y species. From the XPS and soft XAS analyses, it can be concluded that the cathode/electrolyte interaction is critically important in determining the CEI properties.

In order to further understand the evolutions of the CEIs formed on LCO electrodes in different electrolytes and their influences on the cathode structures, cycled LCO cathodes were characterized by scanning tunneling electron microscopy (STEM). Both the high-angle annular dark-field (HAADF) and annular bright-field (ABF) images are shown in **Figure 4**. In the BL-carbonate electrolyte, the LCO cathode is covered by CEI with a thickness of 7–11 nm after just 100 cycles under 4.5 V (Figure 4a). Within the CEI, crystalline domains with an interlayer distance of ≈0.47 nm are found, which resemble the bulk layered structure but with different orientations. It is likely due to the dissolution of Co ions, which results from the catalytic decomposition of the BL-carbonate electrolyte and the associated generation of corrosive side products. Some Co ions can precipitate in the form of Co oxides as part of the CEI. From the HAADF image, it is clear that such corrosion greatly changes the crystalline structure on the LCO surface (Figure 4b). The top surface (at least 5 nm thick) transforms from the original layered structure to a rock-salt structure, which would hinder the interfacial charge transfer processes, as evidenced by the

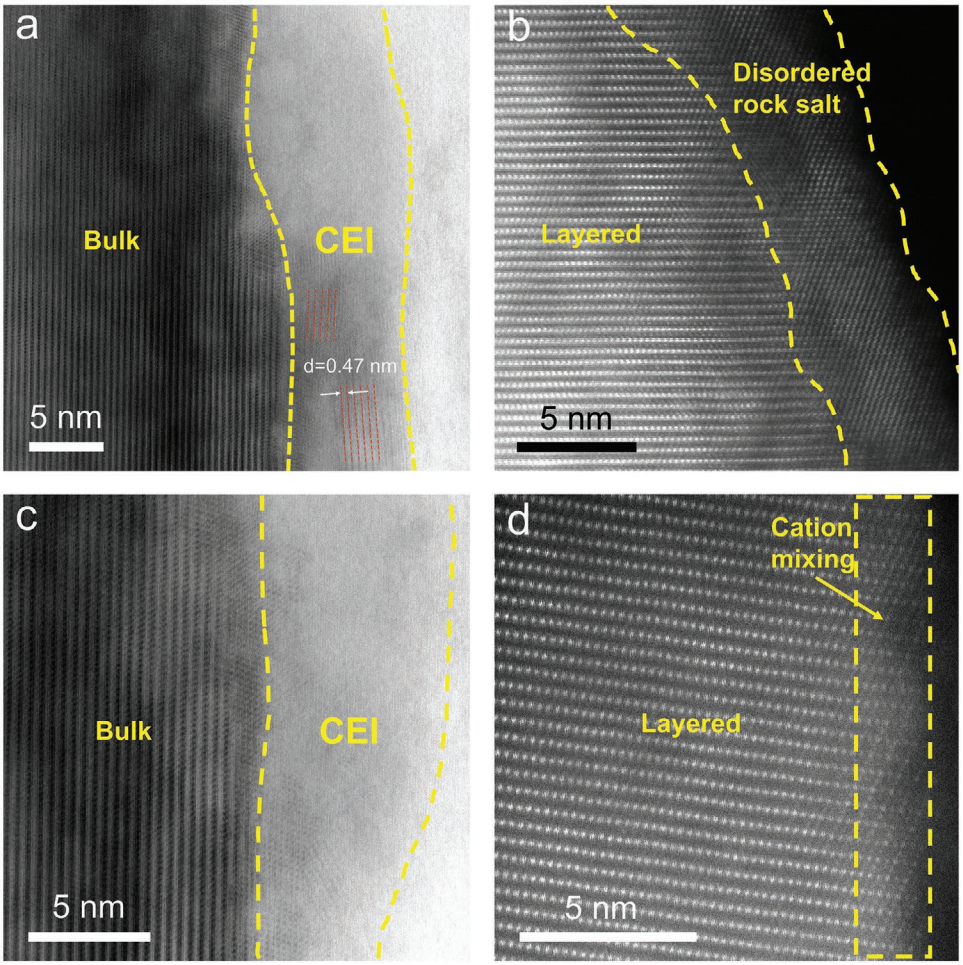

Figure 4. The CEI structures on cycled LCO cathodes in different electrolytes by HR-STEM characterizations. a,b) After 100 cycles in the BL-carbonate electrolyte. c,d) After 300 cycles in the AD-ether electrolyte. a,c) The ABF-STEM images. b,d) The HAADF-STEM images.

impedance spectroscopy (Figure 2i). Nevertheless, the cathode degradation in the AD-ether electrolyte is significantly suppressed, as shown in the STEM images of LCO after 300 cycles. Despite the CEI layer grows to 5–8 nm after long-term cycling (Figure 4c), the presence of heavy transition metal Co ions in the CEI is much less than those in the BL-carbonate electrolyte. It is likely that there is limited Co ion dissolution during the initial CEI formation process due to reactive intermediates from electrolyte oxidation, which is greatly inhibited with the CEI in place. As a result, the surface structure of the LCO cathode shows very limited signs of cation mixing (≈2 nm) after 300 cycles under 4.5 V. This result clearly manifests that improving the CEI could greatly enhance the LCO cycling stability under high voltage.

In this work, we have demonstrated that designing an in situ formed advanced CEI on the LCO cathode is highly effective in achieving its long-term cycling performance under high voltage (4.5 V) and elevated temperature (55 °C). The AD-ether electrolyte not only has an excellent compatibility with the Li metal anode due to the in situ formed stable SEI, but more importantly enables the formation of a F-enriched CEI to inhibit interfacial parasitic reactions and protect the LCO cathode. Besides, the practical applicability of the Li||LCO battery under high rate and low-temperature conditions is also improved with the AD-ether electrolyte. Our results highlight a promising strategy for realizing high-energy-density LCO-based batteries and shed light on holistic design of electrode/electrolyte interphases on highly-demanding electrode materials.

Supporting Information

Supporting Information is available from the Wiley Online Library or from the author.

Acknowledgements

X.R. and X.Z. contributed equally to this work. This work was supported by the Assistant Secretary for Energy Efficiency and Renewable Energy, Vehicle Technologies Office of the U.S. Department of Energy (DOE) through the Advanced Battery Materials Research (BMR) program (Battery500 Consortium) under the Contract No. DE-AC05-76RL01830 for Pacific Northwest National Laboratory (PNNL) and Contract No. DE-SC0012704 for Brookhaven National Laboratory (BNL). The microscopic and XPS spectroscopic characterizations were performed using EMSL

(grid. 436923.9), a DOE Office of Science User Facility sponsored by the Office of Biological and Environmental Research located at PNNL. TEM sample preparation and cross-section SEM imaging was performed in the Radiological Microscopy Suite (RMS), located in the Radiochemical Processing Laboratory (RPL) at PNNL. PNNL is operated by Battelle for the DOE under Contract DE-AC05-76RL01830. This research used resources at beamlines 7-BM (QAS) and 23-ID-2 (IOS) of the National Synchrotron Light Source II, a U.S. Department of Energy (DOE) Office of Science User Facility operated for the DOE Office of Science by BNL under Contract DE-SC0012704. Laminated LCO cathode sheets were obtained from the Cell Analysis, Modeling, and Prototyping (CAMP) Facility at Argonne National Laboratory. The salt LiFSI was provided by Dr. Kazuhiko Murata of Nippon Shokubai Co., Ltd.

Conflict of Interest

The authors declare no conflict of interest.

Keywords

cathode/electrolyte interphases, ether electrolytes, high-voltage $LiCoO_2$, lithium metal batteries

[1] a) M. Winter, B. Barnett, K. Xu, *Chem. Rev.* **2018**, *118*, 11433; b) J. Xie, Y. C. Lu, *Nat. Commun.* **2020**, *11*, 2499.

[2] L. Wang, B. Chen, J. Ma, G. Cui, L. Chen, *Chem. Soc. Rev.* **2018**, *47*, 6505.

[3] Q. Liu, X. Su, D. Lei, Y. Qin, J. G. Wen, F. M. Guo, Y. M. A. Wu, Y. C. Rong, R. H. Kou, X. H. Xiao, F. Aguesse, J. Bareno, Y. Ren, W. Q. Lu, Y. X. Li, *Nat. Energy* **2018**, *3*, 936.

[4] D. Aurbach, B. Markovsky, A. Rodkin, E. Levi, Y. S. Cohen, H. J. Kim, M. Schmidt, *Electrochim. Acta* **2002**, *47*, 4291.

[5] J. Kikkawa, S. Terada, A. Gunji, T. Nagai, K. Kurashima, K. Kimoto, *J. Phys. Chem. C* **2015**, *119*, 15823.

[6] Z. Zhu, D. Yu, Z. Shi, R. Gao, X. Xiao, I. Waluyo, M. Ge, Y. Dong, W. Xue, G. Xu, W.-K. Lee, A. Hunt, J. Li, *Energy Environ. Sci.* **2020**, *13*, 1865.

[7] P. Yan, J. Zheng, Z. K. Tang, A. Devaraj, G. Chen, K. Amine, J. G. Zhang, L. M. Liu, C. Wang, *Nat. Nanotechnol.* **2019**, *14*, 602.

[8] a) S. Kalluri, M. Yoon, M. Jo, S. Park, S. Myeong, J. Kim, S. X. Dou, Z. Guo, J. Cho, *Adv. Energy Mater.* **2017**, *7*, 1601507; b) Z. Yang, R. Li, Z. Deng, *Sci. Rep.* **2018**, *8*, 863; c) C. Wang, T. Wang, L. Wang, Z. Hu, Z. Cui, J. Li, S. Dong, X. Zhou, G. Cui, *Adv. Sci.* **2019**, *6*, 1901036; d) S. Lin, J. Zhao, *ACS Appl. Mater. Interfaces* **2020**, *12*, 8316; e) T. Dong, J. Zhang, G. Xu, J. Chai, H. Du, L. Wang, H. Wen, X. Zang, A. Du, Q. Jia, X. Zhou, G. Cui, *Energy Environ. Sci.* **2018**, *11*, 1197; f) L. Shao, L. Zhou, L. Yang, C. Jia, C. Wang, S. Hu, X. Zeng, C. Yang, C. Huang, Y. Zhou, X. Xi, *Electrochim. Acta* **2019**, *297*, 742; g) J. Qian, L. Liu, J. Yang, S. Li, X. Wang, H. L. Zhuang, Y. Lu, *Nat. Commun.* **2018**, *9*, 4918; h) M. Zhang, J. Zhang, J. Yang, X. Du, Z. Chen, K. Chen, C. Lu, H. Zhang, T. Dong, J. Li, Z. Zhang, H. Zhang, G. Cui, *J. Electrochem. Soc.* **2019**, *166*, A2313; i) K. H. Nie, X. R. Sun, J. Y. Wang, Y. Wang, W. B. Qi, D. D. Xiao, J. N. Zhang, R. J. Xiao, X. Q. Yu, H. Li, X. J. Huang, L. Q. Chen, *J. Power Sources* **2020**, *470*, 228423.

[9] J. Y. Liang, X. D. Zhang, X. X. Zeng, M. Yan, Y. X. Yin, S. Xin, W. P. Wang, X. W. Wu, J. L. Shi, L. J. Wan, Y. G. Guo, *Angew. Chem., Int. Ed. Engl.* **2020**, *59*, 6585.

[10] a) J. Liu, Z. N. Bao, Y. Cui, E. J. Dufek, J. B. Goodenough, P. Khalifah, Q. Y. Li, B. Y. Liaw, P. Liu, A. Manthiram, Y. S. Meng, V. R. Subramanian, M. F. Toney, V. V. Viswanathan, M. S. Whittingham, J. Xiao, W. Xu, J. H. Yang, X. Q. Yang, J. G. Zhang, *Nat. Energy* **2019**, *4*, 180; b) W. Xu, J. Wang, F. Ding, X. Chen, E. Nasybulin, Y. Zhang, J.-G. Zhang, *Energy Environ. Sci.* **2014**, *7*, 513; c) X.-Y. Yue, X.-L. Li, W.-W. Wang, D. Chen, Q.-Q. Qiu, Q.-C. Wang, X.-J. Wu, Z.-W. Fu, Z. Shadike, X.-Q. Yang, Y.-N. Zhou, *Nano Energy* **2019**, *60*, 257; d) X.-Y. Yue, W.-W. Wang, Q.-C. Wang, J.-K. Meng, X.-X. Wang, Y. Song, Z.-W. Fu, X.-J. Wu, Y.-N. Zhou, *Energy Storage Mater.* **2019**, *21*, 180.

[11] a) D. Lin, Y. Liu, Y. Cui, *Nat. Nanotechnol.* **2017**, *12*, 194; b) X. B. Cheng, R. Zhang, C. Z. Zhao, Q. Zhang, *Chem. Rev.* **2017**, *117*, 194.

[12] a) S. Chen, J. Zheng, D. Mei, K. S. Han, M. H. Engelhard, W. Zhao, W. Xu, J. Liu, J. G. Zhang, *Adv. Mater.* **2018**, *30*, 1706102; b) J. Zheng, S. Chen, W. Zhao, J. Song, M. H. Engelhard, J.-G. Zhang, *ACS Energy Lett.* **2018**, *3*, 315; c) X. D. Ren, S. R. Chen, H. Lee, D. H. Mei, M. H. Engelhard, S. D. Burton, W. G. Zhao, J. M. Zheng, Q. Y. Li, M. S. Ding, M. Schroeder, J. Alvarado, K. Xu, Y. S. Meng, J. Liu, J. G. Zhang, W. Xu, *Chem* **2018**, *4*, 1877; d) H. Jia, L. Zou, P. Gao, X. Cao, W. Zhao, Y. He, M. H. Engelhard, S. D. Burton, H. Wang, X. Ren, Q. Li, R. Yi, X. Zhang, C. Wang, Z. Xu, X. Li, J. G. Zhang, W. Xu, *Adv. Energy Mater.* **2019**, *9*, 1900784; e) W. J. Kwak, H. S. Lim, P. Gao, R. Feng, S. Chae, L. Zhong, J. Read, M. H. Engelhard, W. Xu, J. G. Zhang, *Adv. Funct. Mater.*, https://doi.org/10.1002/adfm.202002927; f) X. Zhang, L. Zou, Y. Xu, X. Cao, M. H. Engelhard, B. E. Matthews, L. Zhong, H. Wu, H. Jia, X. Ren, P. Gao, Z. Chen, Y. Qin, C. Kompella, B. W. Arey, J. Li, D. Wang, C. Wang, J. G. Zhang, W. Xu, *Adv. Energy Mater.* **2020**, *10*, 2000368.

[13] X. Ren, L. Zou, X. Cao, M. H. Engelhard, W. Liu, S. D. Burton, H. Lee, C. Niu, B. E. Matthews, Z. Zhu, C. Wang, B. W. Arey, J. Xiao, J. Liu, J.-G. Zhang, W. Xu, *Joule* **2019**, *3*, 1662.

[14] a) X. Ren, L. Zou, S. Jiao, D. Mei, M. H. Engelhard, Q. Li, H. Lee, C. Niu, B. D. Adams, C. Wang, J. Liu, J.-G. Zhang, W. Xu, *ACS Energy Lett.* **2019**, *4*, 896; b) L. Suo, W. Xue, M. Gobet, S. G. Greenbaum, C. Wang, Y. Chen, W. Yang, Y. Li, J. Li, *Proc. Natl. Acad. Sci. USA* **2018**, *115*, 1156; c) X. Fan, L. Chen, X. Ji, T. Deng, S. Hou, J. Chen, J. Zheng, F. Wang, J. Jiang, K. Xu, C. Wang, *Chem* **2018**, *4*, 174.

[15] a) T. Li, X.-Q. Zhang, P. Shi, Q. Zhang, *Joule* **2019**, *3*, 2647; b) C. Wang, Y. S. Meng, K. Xu, *J. Electrochem. Soc.* **2018**, *166*, A5184.

[16] X. Cao, X. Ren, L. Zou, M. H. Engelhard, W. Huang, H. Wang, B. E. Matthews, H. Lee, C. Niu, B. W. Arey, Y. Cui, C. Wang, J. Xiao, J. Liu, W. Xu, J.-G. Zhang, *Nat. Energy* **2019**, *4*, 796.

[17] a) Y. Yu, P. Karayaylali, Y. Katayama, L. Giordano, M. Gauthier, F. Maglia, R. Jung, I. Lund, Y. Shao-Horn, *J. Phys. Chem. C* **2018**, *122*, 27368; b) M. Gauthier, P. Karayaylali, L. Giordano, S. Feng, S. F. Lux, F. Maglia, P. Lamp, Y. Shao-Horn, *J. Electrochem. Soc.* **2018**, *165*, A1377.

[18] M. Balasubramanian, H. S. Lee, X. Sun, X. Q. Yang, A. R. Moodenbaugh, J. McBreen, D. A. Fischer, Z. Fu, *Electrochem. Solid-State Lett.* **2002**, *5*, A22.